Multi-objective Bayesian global optimization for continuous problems and applications

Yang, K.

Chapter 7

Applications

This chapter presents and analyses an engineered expected hypervolume improvement (EHVI) algorithm, which aims to solve the problem of PID parameter tuning and the optimization problem of controlling the substrate feed of a bio-gas plant. The EHVI is the expected value of the increment of the hypervolume indicator given a Pareto front approximation and a predictive multivariate Gaussian distribution of a new point. To solve this problem, $\mathcal{S}$-metric selection-based efficient global optimization (SMS-EGO), EHVI based efficient global optimization (EHVI-EGO) and SMS-EMOA are used and compared in both the PID parameter tuning problem and for bio-gas plant feed optimization. The results of the experiments show that surrogate model based algorithms perform better than SMS-EMOA, and the performance of EHVI-EGO is slightly better than SMS-EGO.

This chapter is structured as follows: Section 7.1 describes the backgrounds of the bio-plant and PID parameter tuning problems. Section 7.2 introduces the PID parameter tuning task, the multi-objective nonlinear model predictive control approach as well as, the biogas process model. Section 7.3 and Section 7.4 discuss experimental studies and results.

7.1 Backgrounds

Based on REN21's (Renewable Energy Policy Network for the 21st Century) 2014 report, renewable energy contributed 19 percent to worldwide energy consumption and 22 percent to worldwide electricity generation in 2012 and 2013,

respectively. Among renewable energy, the use of renewable energy in the form of biogas grew at a rapid pace in the past decade. Biogas is produced in bio-gas plants, where an anaerobic degradable substrate is decomposed by anaerobic bacteria in an oxygen-free environment. The main ingredient of biogas is methane, which can be used for further utilization, such as energy production.

Maximizing the yield and maintaining the bio-gas plant stability are crucial for commercial use. To this ends, bio-gas plants should work at optimal operating points. This can be achieved by adjusting the substrate mixture and by tracking the optimal setpoints [105]. However, due to the high dimensional nonlinearity of the anaerobic digestion process and due to lacking reliable measurement sensors on most full-scale bio-gas plants [106], predicting the biogas throughput and designing the optimal feedback control are challenging tasks in the field of anaerobic digestion.

Batstone et al. [107] proposed the Anaerobic Digestion Model No.1 (ADM1) in 2002, and we use it as dynamic simulation model in multi-objective nonlinear model predictive control (MONMPC). In MONMPC, there is an upper-level controller which generates the optimal methane setpoint and the corresponding optimal substrate feed that is passed through to a lower-level controller, which tracks a directly measurable process value (or setpoint). MONMPC is chosen due to the multi-objective nature of bio-gas plant operation, *maximizing the profits* and *minimizing the ecological footprint* [43].

For multi-objective black-box optimization, many algorithms exist. Evolutionary algorithms for solving these problems exist, e.g., NSGA-II [75] and SMS-EMOA [19], which, however, typically require many function evaluations ($\gg 1000$) to find good approximations to Pareto fronts. In controller optimization, expensive evaluations of black-box objective functions pose typical challenges. In this chapter, we focus, therefore, on optimization with a small budget of function evaluations and use surrogate-model based optimization strategies [108], which replace exact evaluations by approximations learned from past evaluations. Recently, this idea has been generalized to multi-objective optimization (e.g. [109, 110, 111]). Algorithms that generalize efficient global optimization are S-Metric Selection EGO (SMS-EGO) [50] and Expected Hypervolume Improvement-based EGO (EHVI-EGO) [42, 60, 61]. Recently, the runtime efficiency of the exact infill criterion in the bi-objective EHVI-EGO was improved from $O(n^3 \log n)$ to $O(n^2)$ [42], where n is the number of points in the archive. This makes it competitive with other techniques that use computable infill criteria, in particular, SMS-EGO.

The specific contributions of this chapter are as follows: In this chapter, we

will compare algorithms in the application domain of controller optimization. In this chapter, we will provide a first application study with the new Fast EHVI-EGO. The contribution of this chapter is also to discuss concisely the definition of multi-objective model-predictive control optimization in bio-gas plant – more precisely for minimizing stage cost and terminal cost of a bio-gas plant – and of multi-objective parameter tuning of PID controllers.

7.2 Problem Definition

7.2.1 PID Parameter Tuning

This benchmark on PID parameter tuning is taken from [112]. The three parameters in PID controller are: proportionality K_p, integral K_i and derivative K_d. The transfer function of PID controller for a continuous system can be defined as: $Y(s) = \frac{U(s)}{E(s)} = K_p + \frac{K_i}{s} + K_d s$, where $E(s)$ and $U(s)$ represent error signal and control signal, respectively. The basic idea of PID controller is attempting to minimize an error ($E(s)$) by adjusting the process control inputs. The process of PID controller can be described as follows: when a setpoint is set or $E(s)$ exists, $E(s)$ will be calculated by the difference between the setpoint and actual output, and a PID controller will generate a new control signal ($U(s)$) based on $E(s)$. Then the new control signal $U(s)$ is applied to the plant model, and the new actual output and $E(s)$ are generated again. The structure of a PID control is shown in Figure 7.1.

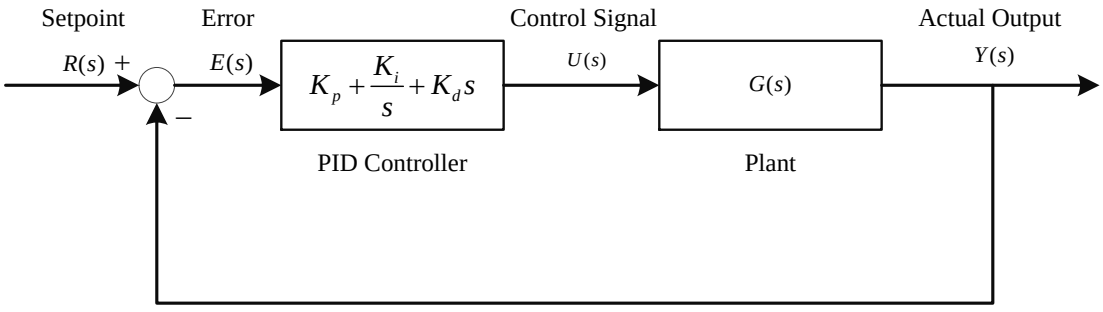

Figure 7.1: The structure of PID control.

Problem and Fitness function The chosen transfer functions modelling the plant in this chapter are:

$$G_1(s) = \frac{25.2s^2 + 21.2s + 3}{s^5 + 16.58s^4 + 25.41s^3 + 17.18s^2 + 11.70s + 1} \tag{2-1}$$

$$G_2(s) = \frac{4.228}{(s + 0.5)(s^2 + 1.64s + 8.456)} \tag{2-2}$$

The step response of these two plants is analyzed with the criteria of *settling time* (t_s) and *percentage overshoot* (PO). *Settling time* (t_s) is defined as time elapsed from the application of an ideal instantaneous step input to the time, at which the output has entered error band with 2% in this chapter, while *percentage overshoot* (PO) refers to the percentage of an output exceeding its final steady-state value.

7.2.2 Robust PID Tuning

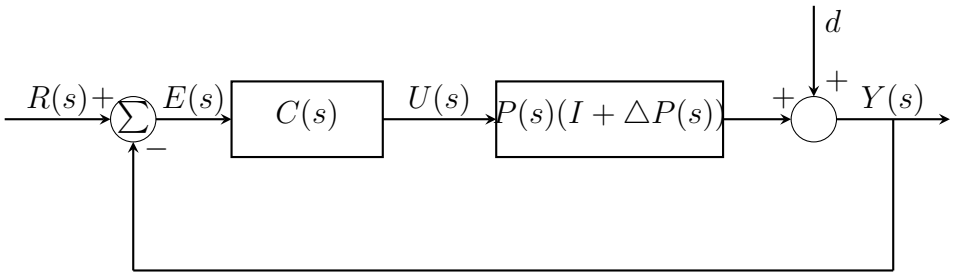

Figure 7.2: Feedback control system with plant perturbation and external disturbance.

The structure of the feedback controller is shown in Fig 7.2, where $R(s)$ is the reference input signal, $E(s)$ represents error signal, $C(s)$ is the transfer function of the controller, $U(s)$ is control signal, $P(s)$ stands for controlled plant, $\triangle P(s)$ is the plant perturbation, $d(t)$ is the external disturbance and $Y(s)$ is the output of the system. For PID controller, three parameters are consisted in $C(s)$: proportionality $B2$, integral $B1$ and derivative $B0$, and the transfer function of PID controller for a continuous system can be defined as: $C(s) = \frac{B_2 s^2 + B_1 s + B_0}{s}$. The basic idea of PID controller is to attempt to minimize an error ($E(s)$) by adjusting the process control inputs.

The benchmark for PID tuning is taken from [113] [114]. The transfer function of the plant is given as follows:

$$P(S) = \begin{pmatrix} \frac{-33.98}{(98.02s+1)(0.42s+1)} & \frac{32.63}{(99.6s+1)(0.35s+1)} \\ \frac{-18.85}{(75.43s+1)(0.30s+1)} & \frac{34.84}{(110.5s+1)(0.03s+1)} \end{pmatrix} \tag{2-3}$$

Objective functions Two criteria were used here: balanced performance criterion $J_\infty = (J_a^2 + J_b^2)^{1/2}$ [115] and interval squared error $J_2 = \int_0^\infty e^T(t)e(t)dt$. For J_∞, J_a and J_b are defined as follows: $J_a^2 = ||W_1(s)T(s)||_\infty$, $J_b^2 = ||W_2(s)S(s)||_\infty$. Here, $W_1(s)$ is the assumed boundary of plant perturbation $\triangle P(s)$, $W_2(s)$ is a stable weighting function matrix and they are defined in [115]:

$$W_1(s) = \frac{100s+1}{s+1000} \times I_{2\times 2}, \tag{2-4}$$

$$W_2(s) = \frac{s+1000}{1000s+1} \times I_{2\times 2}. \tag{2-5}$$

$T(s)$ and $S(s)$ are the sensitivity and complementary sensitivity functions of the system, respectively, and they can be calculated by:

$$S(s) = (I + P(s)C(s))^{-1}, \tag{2-6}$$

$$T(s) = P(s)C(s)(I + P(s)C(s))^{-1}. \tag{2-7}$$

7.2.3 Bio-gas Plant Optimization

Consider a bio-gas plant fed with $n_\mathrm{u} \in \mathbb{N}$ substrates. Its $n_\mathrm{s} \in \mathbb{N}$ dimensional system state is symbolized by $\boldsymbol{x} : \mathbb{R}_0^+ \to \mathcal{S}$ and its substrate feed by $\boldsymbol{u} : \mathbb{R}_0^+ \to \mathcal{U}$, with $\mathcal{S} \subseteq \mathbb{R}^{n_\mathrm{s}}$ and $\mathcal{U} \subseteq \mathbb{R}^{n_\mathrm{u}}$ denoting the state and input space, respectively. In multi-objective nonlinear model predictive control, a time dependent ($t \in \mathbb{R}_0^+$) optimization problem that is defined over a prediction horizon $T_\mathrm{p} \in \mathbb{R}^+$ is solved at every discrete time instant $t_k := k \cdot \delta$, with sampling time $\delta \in \mathbb{R}^+$ and $k = 0, 1, 2, \ldots$, [116]. The objective is to minimize a two-dimensional objective function $\boldsymbol{J} : \mathcal{S} \times \mathcal{U} \to \mathbb{R}^2$, which depends on the open loop state ${}^o\boldsymbol{s} : \mathbb{R}_0^+ \to \mathcal{S}$ and the open loop substrate feed ${}^o\boldsymbol{u} : \mathbb{R}_0^+ \to \mathcal{U}$ of the controlled bio-gas plant, approximately modeled by a set of nonlinear differential equations ${}^o\boldsymbol{s}'(t) = \boldsymbol{f}\,({}^o\boldsymbol{s}(t), \boldsymbol{u}(t))$, called the bio-gas plant model $\boldsymbol{f} : \mathcal{S} \times \mathcal{U} \to \mathbb{R}^{n_\mathrm{s}}$. The optimization problem is solved by choosing the optimal substrate feed ${}^o\boldsymbol{u}$ over a control horizon $T_\mathrm{c} \in \mathbb{R}^+$, $\delta \leq T_\mathrm{c} \leq T_\mathrm{p}$. The MONMPC problem can be stated as

follows:

$$
\begin{aligned}
&\text{For each } k = 0, 1, 2, \dots \text{ set } t_k = k \cdot \delta \text{ and solve:} \\
&\quad \min_{{}^{o}\boldsymbol{u}(\cdot)\in\mathcal{U}} \boldsymbol{J}\left({}^{o}\boldsymbol{s}(\tau), {}^{o}\boldsymbol{u}(\tau)\right) \\
&\text{s.t. } {}^{o}\boldsymbol{s}'(\tau) = \boldsymbol{f}\left({}^{o}\boldsymbol{s}(\tau), {}^{o}\boldsymbol{u}(\tau)\right), \\
&\quad {}^{o}\boldsymbol{s}\left(t_k\right) = \boldsymbol{x}\left(t_k\right), \\
&\quad {}^{o}\boldsymbol{s}(\tau) \in \mathcal{S}, \forall \tau \in \left[t_k, t_k + T_\mathrm{p}\right], \\
&\quad {}^{o}\boldsymbol{u} : \left[t_k, t_k + T_\mathrm{c}\right] \to \mathcal{U}, \\
&\quad {}^{o}\boldsymbol{u}(\tau) = {}^{o}\boldsymbol{u}\left(t_k + T_\mathrm{c}\right), \forall \tau \in \left(t_k + T_\mathrm{c}, t_k + T_\mathrm{p}\right].
\end{aligned}
\tag{2-8}
$$

Since the objective function, i. e. $\boldsymbol{J} := (J_1, J_2)^T$, is vector valued, there is not one single optimal solution, but rather many trade-off solutions, which are all Pareto optimal with respect to (2-8) and collected in the so-called Pareto optimal set $\mathcal{P}_k^* \subset \mathcal{U}$, [117]. The trade-off solution applied to the plant, ${}^{o}\boldsymbol{u}_k^*$, is given by a weighted sum, $\varpi_1, \varpi_2 \in \mathbb{R}$:

$${}^{o}\boldsymbol{u}_k^* := \arg\min_{{}^{o}\boldsymbol{u}\in\mathcal{P}_k^*} \sum_{i_\mathrm{o}=1}^{2} \varpi_{i_\mathrm{o}} \cdot J_{i_\mathrm{o}}\left({}^{o}\boldsymbol{s}, {}^{o}\boldsymbol{u}\right), \tag{2-9}$$

and then applied for the duration of the sampling time δ:

$$\boldsymbol{u}(t) = {}^{o}\boldsymbol{u}_k^*(t), \qquad t \in \left[t_k, t_k + \delta\right). \tag{2-10}$$

Objective functions The objective function components J_1 and J_2 are defined as follows. The first component of the objective function is defined as:

$$J_1 := \frac{1}{T_\mathrm{p}} \cdot \int_{t_k}^{t_k+T_\mathrm{p}} F_1(\tau)\ \mathrm{d}\tau + T_{\mathrm{p},1}, \tag{2-11}$$

It is the average of the negative financial profit $E_\mathrm{plant} := (\text{benefit} - \text{cost})$ obtained by operating the bio-gas plant over the prediction horizon T_p, with the first component of the stage cost defined as:

$$F_1(\tau) := -E_\mathrm{plant}\left({}^{o}\boldsymbol{s}(\tau), {}^{o}\boldsymbol{u}(\tau)\right). \tag{2-12}$$

The cost function is defined by the sum of the substrate and energy costs and the benefit function is defined by the profit obtained after selling the produced electrical and thermal energy, which, in Germany, is determined by the Renewable Energy Sources Act - EEG [118]. The minus sign in eq. (2-12) is added because the optimization problem in eq. (2-8) is formulated as a minimization problem.

In eq. (2-11) the first component of the terminal cost $T_{\mathrm{p},1}$ is used, which is defined as:

$$T_{\mathrm{p},1} := \kappa_{T,1} \cdot F_1 \left(t_k + T_{\mathrm{p}} \right), \tag{2-13}$$

with the weighting factor $\kappa_{T,1} \in \mathbb{R}^+$.

The second component of the objective function J_2,

$$J_2 := \frac{1}{T_{\mathrm{p}}} \cdot \int_{t_k}^{t_k+T_{\mathrm{p}}} F_2(\tau) \, \mathrm{d}\tau + \int_{t_k}^{t_k+T_{\mathrm{p}}} \left\| {}^{o}\boldsymbol{u}'(\tau) \right\|_2^2 \, \mathrm{d}\tau + T_{\mathrm{p},2} \quad , \tag{2-14}$$

contains a weighted sum of all $n_{\mathrm{c}} \in \mathbb{N}_0$ boundary conditions that are active over the prediction horizon T_{p}, defined in the second component of the stage cost F_2:

$$F_2(\tau) := \sum_{i_{\mathrm{c}}=1}^{n_{\mathrm{c}}} \kappa_{i_{\mathrm{c}}} \cdot \mathrm{bound}_{i_{\mathrm{c}}} \left({}^{o}\boldsymbol{s}(\tau), {}^{o}\boldsymbol{u}(\tau) \right). \tag{2-15}$$

Furthermore, J_2 contains the integral over the change of the open loop control input ${}^{o}\boldsymbol{u}$ and the terminal penalty term $T_{\mathrm{p},2}$ with the weighting factor $\kappa_{T,2} \in \mathbb{R}^+$:

$$T_{\mathrm{p},2} := \kappa_{T,2} \cdot F_2 \left(t_k + T_{\mathrm{p}} \right). \tag{2-16}$$

In eq. (2-15) the weights $\kappa_{i_{\mathrm{c}}} \in \mathbb{R}^+$ are normalized, $\sum_{i_{\mathrm{c}}}^{n_{\mathrm{c}}} \kappa_{i_{\mathrm{c}}} = 1$, and the boundary conditions are defined as:

$$\mathrm{bound}_{i_{\mathrm{c}}} : \mathcal{S} \times \mathcal{U} \to \begin{cases} 0 < \cdots \leq \left(1 \text{ or } \frac{4.6851^2}{6} \right) & \text{if active,} \\ 0 & \text{else.} \end{cases} \tag{2-17}$$

Such that all constraints are smooth, some of the them are implemented using the Tukey biweight function $\rho_{\mathrm{T}} : \mathbb{R} \to \mathbb{R}^+$, which is defined as, with $C_{\mathrm{T}} := 4.6851$ [119]:

$$\rho_{\mathrm{T}} \left(u_{\mathrm{T}} \right) := \begin{cases} \frac{C_{\mathrm{T}}^2}{6} \left[1 - \left(1 - \left(\frac{u_{\mathrm{T}}}{C_{\mathrm{T}}} \right)^2 \right)^3 \right] & |u_{\mathrm{T}}| \leq C_{\mathrm{T}}, \\ \frac{C_{\mathrm{T}}^2}{6} & \text{else.} \end{cases} \tag{2-18}$$

In eq. (2-18), $u_{\mathrm{T}} \in \mathbb{R}$ must be replaced by the difference between the constrained value and its boundary condition.

Examples for the n_{c} constraint functions $\mathrm{bound}_{i_{\mathrm{c}}}$, $i_{\mathrm{c}} = 1, \ldots, n_{\mathrm{c}}$, are upper and lower boundaries for VFA/TA, COD degradation rate, pH value, OLR, HRT, NH_4-N and VFA (for details see [43]).

Bio-gas Process:

In the simulation experiments performed in this chapter, a model of a bio-gas plant is used. This model and the real plant are described here. The modeled bio-gas plant is a full-scale agricultural bio-gas plant with an electrical power of 500 kW, located in Germany. The plant is configured as a two-stage system with a primary digester (1st) ($V_{\text{liq}} = 1977$ m^3) and a secondary (or post) digester ($V_{\text{liq}} = 4182$ m^3), whereas the secondary digester also serves as a final storage tank. A pumping station offers the possibility of interchanging sludge between both digesters. The first digester is mainly fed with maize silage, swine, and cattle manure as well as grass silage. The secondary digester is not fed. The produced biogas is burned in two CHPs with an electrical power of 250 kW each. The produced electrical power is injected into the local grid, which is enumerated by the EEG 2009. Both digesters are heated with the thermal energy produced by the CHPs and are operated at about 40 ^{o}C.

The simulation model is implemented in MATLAB® in a self-developed toolbox, which is freely available under the terms of the GNU GPL.

7.3 Experimental Settings

PID Parameter Tuning For the PID controller problem, the following parameters were used. The search space for the three parameters (K_p, K_i and K_d) in $G_1(s)$ [120] and $G_2(s)$ [112] is shown in Table 7.1.

Table 7.1: Parameter setting.

	G_1(s)			G_2(s)		
	SMS-EMOA	SMS-EGO	EHVI-EGO	SMS-EMOA	SMS-EGO	EHVI-EGO
K_p	[0,10]	[0,10]	[0,10]	[0,10]	[0,10]	[0,10]
K_i	[0,13]	[0,13]	[0,13]	[0,6]	[0,6]	[0,6]
K_d	[0,18]	[0,18]	[0,18]	[0,6]	[0,6]	[0,6]
n_{pop}	30	32	32	30	32	32
n_{eval}	90	50	50	90	50	50

Robust PID tuning The parameters for the algorithms are shown in Table 7.2.

Table 7.2: Parameter settings.

Algorithm	μ/Initial Population	λ	iteration	pc	pm
EHVI-EGO	30	/	200	/	/
TEHVI-EGO	30	/	200	/	/
NSGA-II	30	30	200	0.9	1/N
SMS-EMOA	30	/	200	0.9	1/N

The TEHVI-EGO boundary ((A, B)) for all the experiments are $(0, \infty)$, except for ZDT3 problem. Since the lower bound of ZDT3 is close to -1, the TEHVI-EGO boundary for ZDT3 was set to $(-1, \infty)$. For the generalized Schaffer problem, the parameter γ was set to $\gamma = 0.4$. All the experiments were repeated five times.

Bio-gas Plant Optimization The simulation of biogas is composed by two stages: intermediate process and steady state. In the first stage, the objective functions are J_1 and J_2 described in section 7.2. For steady state, the objective functions are F_1 and F_2 described in section 7.2. Three different initial substrate feeds, as shown in Table 7.3, were set to test whether the MONMPC is robust against initial substrate feed. SMS-EGO and EHVI-EGO were used and compared, the parameters of these two algorithms can be found in Table 7.3, where T_p, T_c and δ are the control parameters and represent prediction horizon, control horizon, and control sampling time, respectively.

7.4 Experimental Results

7.4.1 PID Parameter Tuning

For PID parameter tuning, the final best and average non-dominated Pareto fronts in the 20 runs are shown in Figures 7.3 and 7.4, where g_1 and g_2 represent *settling time* (t_s) and *percentage overshoot* (PO), respectively. The search space for $G_1(s)$ and $G_2(s)$ are described in Table 7.1.

Figures 7.3 and 7.4 refer to the best and the average Pareto fronts in all runs respectively, and these are generated by using attainment curves of toolbox *plotatta* [34, 36].

Table 7.3: Parameter sets for all experiments.

Component	Test A	Test B	Test C	LB	UB	unit
Q_{maize}	15	5	40	0	30	m^3/d
Q_{manure}	10	5	30	5	15	m^3/d
Q_{grass}	2	0	10	0	30	m^3/d
Exp. no.	T_p/d	T_c/[d]	δ/[d]	n_{pop}	n_{eval}	Method
1	150	10	10	32	50	SMS-EGO
2	150	10	10	32	40	SMS-EGO
3	150	10	10	32	60	SMS-EGO
4	150	10	10	32	50	EHVI-EGO
5	150	10	10	32	40	EHVI-EGO
6	150	10	10	32	60	EHVI-EGO
7	150	10	10	20	60	SMS-EMOA
8	150	10	10	25	75	SMS-EMOA
9	150	10	10	20	80	SMS-EMOA

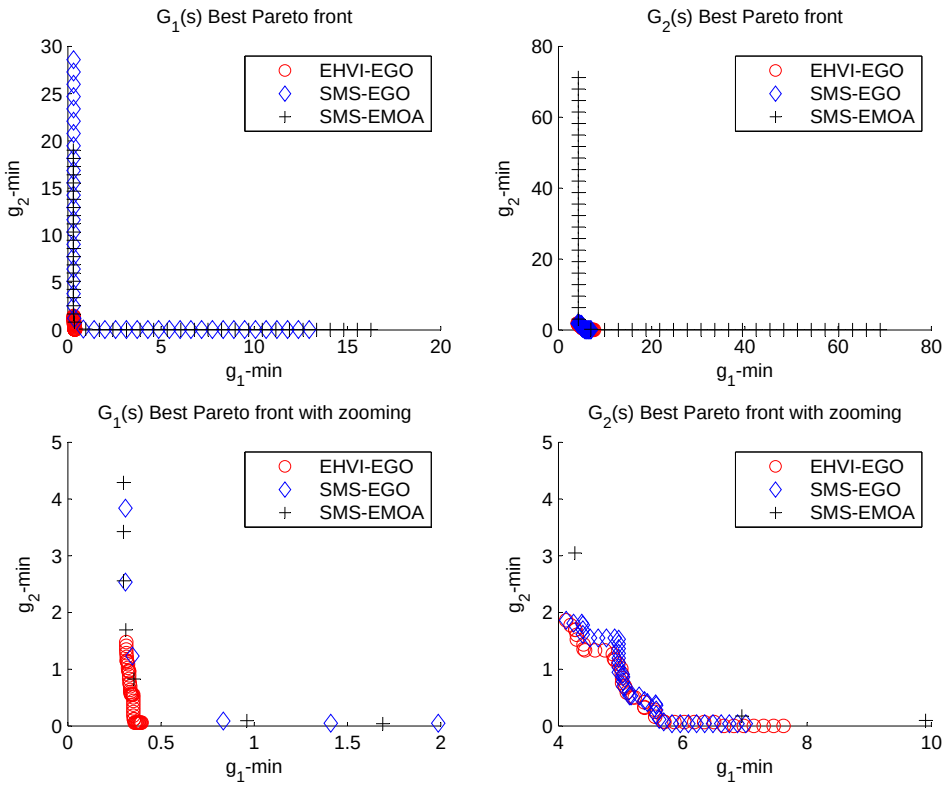

Figure 7.3: Best Pareto fronts.

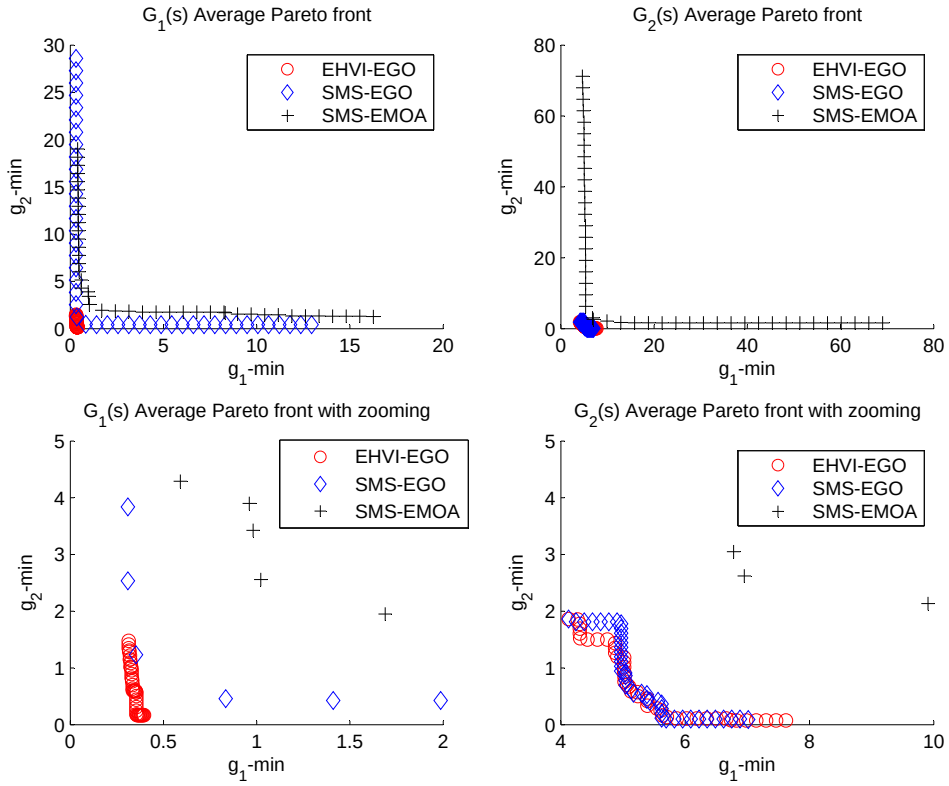

Figure 7.4: Average Pareto fronts.

Comparing the best Pareto fronts generated by surrogate-model-based algorithms and model-free algorithm in Figure 7.3, almost all the elements in SMS-EMOA best Pareto front are dominated by those generated by SMS-EGO and EHVI-EGO, and surrogate model based algorithms (EHVI-EGO and SMS-EGO) outperform model-free algorithm (SMS-EMOA). Comparing the best Pareto front generated by the EHVI-EGO and SMS-EGO in $G_1(s)$ and $G_2(s)$, EHVI-EGO is slightly more robust to reach the "ideal" Pareto front as close as possible than the SMS-EGO.

The difference between best and average Pareto fronts in EHVI-EGO and SMS-EGO are not obviously. This means that when compared to model-free optimization algorithms, surrogate-model-based algorithms can faster converge to the "ideal" Pareto front with fewer evaluations, and EHVI-EGO is more robust to converge than SMS-EGO within a certain number of evaluations.

For statistic analysis, hypervolume in all the experiments are analysed in Table 7.4. The reference points for $G_1(s)$ and $G_2(s)$ in Table 7.4 are [5 5] and [10,5], respectively.

Table 7.4: HV Comparison.

	$G_1(s)$				$G_2(s)$			
	AVG	MIN	MAX	σ	AVG	MIN	MAX	σ
EHVI-EGO	23.38	23.33	23.40	0.02	27.34	26.87	27.62	0.25
SMS-EGO	21.26	14.03	23.37	3.45	27.23	26.04	27.48	0.32
SMS-EMOA	18.95	13.11	22.50	2.81	19.01	3.08	27.49	7.26

From Table 7.4, surrogate-model-based algorithms are more robust compared to a model-free algorithm (SMS-EMOA). EHVI-EGO provides a higher average value of HV and lower value of corresponding standard deviation than those of the other two algorithms. Therefore, in the case of PID parameter tuning problem, EHVI-EGO is more robust and performs better than SMS-EGO and SMS-EMOA.

Figures 7.5 and 7.6 show the step response for $G_1(s)$ and $G_2(s)$. In Figure 7.3, each set of PID parameters corresponds to the first suggested point sorted by NSGA-II [75]. The computation time t_s, corresponds with EHVI-EGO is faster than that of SMS-EGO and SMS-EMOA, and *PO* using EHVI-EGO is also smaller than the other two algorithms.

7.4.2 Robust PID Tuning

Table 7.5: Robust PID parameter tuning.

Test Function	Methods	reference point	Pareto front size				HV			
			max	min	mean	std	max	min	mean	std
PID	EHVI-EGO	[30 2]	6	3	4.6	1.1402	53.7859	32.5078	47.4223	8.6584
PID	TEHVI-EGO	[30 2]	5	3	4.2	0.8367	**53.9046**	38.6312	**49.0419**	6.3154
PID	NSGA-II	[30 2]	54	36	**45**	8.3066	28.0222	27.9868	28.0054	0.0142
PID	SMS-EMOA	[30 2]	9	1	5.2	3.0332	53.3783	27.4147	36.8671	11.8578

Table 7.5 shows the result of the robust PID parameter tuning problem. Figure 7.7 shows the best Pareto fronts of each method for this problem. It shows that TEHVI-EGO can explore more non-dominated candidates than the other algorithms, and almost all the other Pareto fronts are dominated by the (red) squared Pareto front of EHVI-EGO.

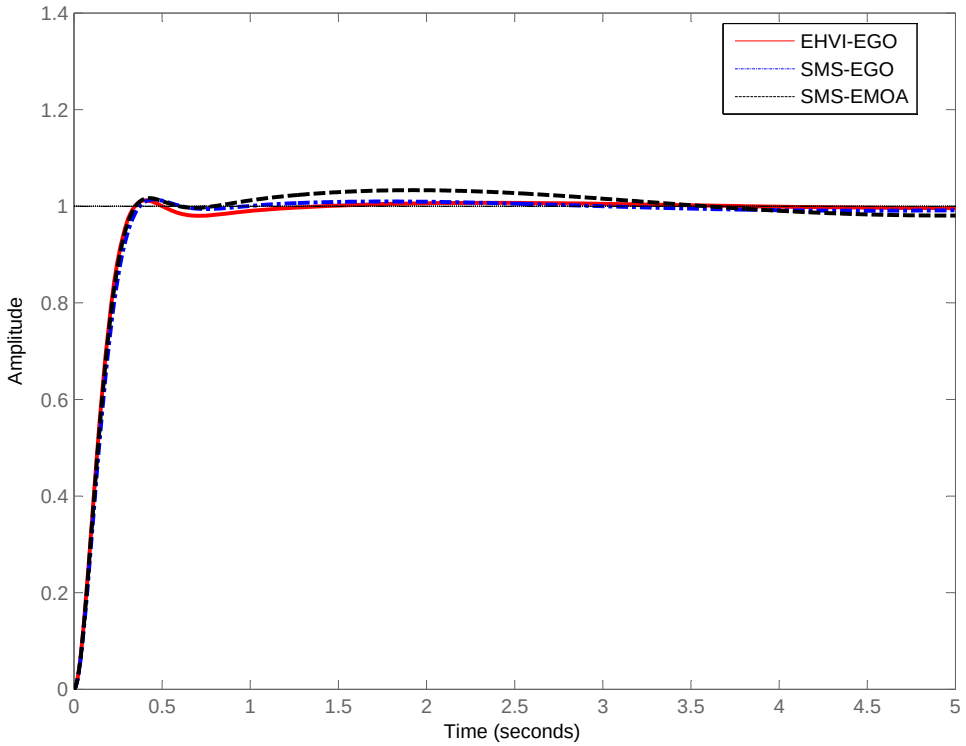

Figure 7.5: $G_1(s)$ step response. For EHVI-EGO $K_p = 1.95$, $K_i = 3.07$, $K_d = 4.61$, for SMS-EGO $K_p = 2.25$, $K_i = 2.92$, $K_d = 4.20$, and for SMS-EMOA $K_p = 2.00$, $K_i = 4.04$, $K_d = 4.48$.

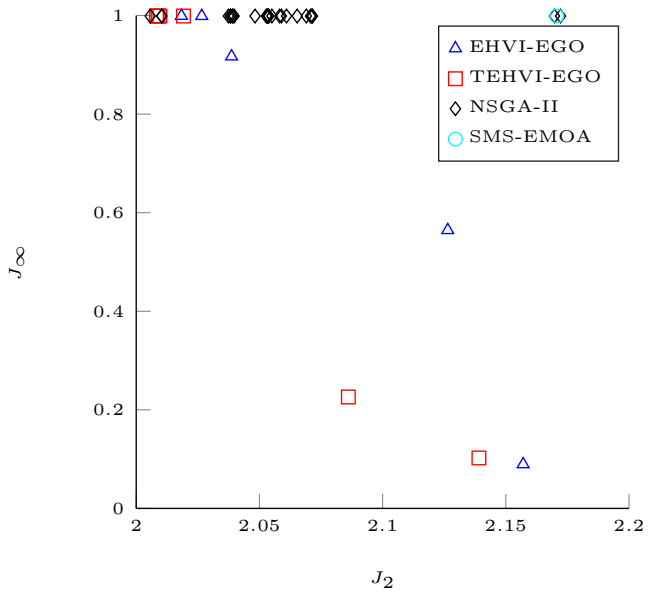

Figure 7.7: The best Pareto fronts for PID problem.

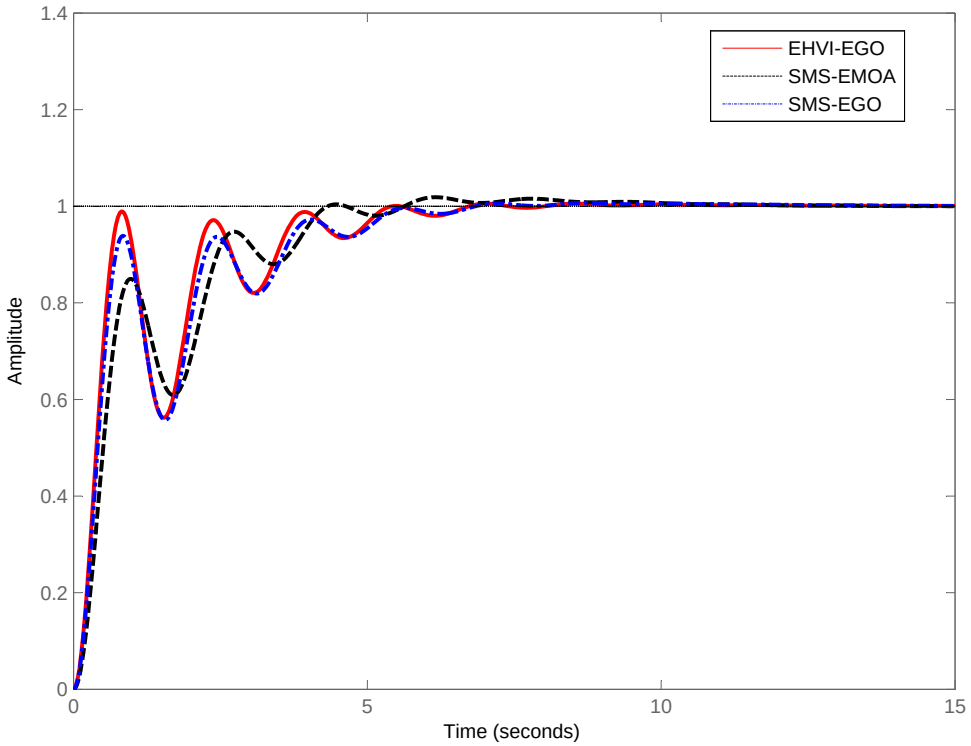

Figure 7.6: $G_2(s)$ step response. For EHVI-EGO $K_p = 2.71$, $K_i = 1.05$, $K_d = 2.13$, for SMS-EGO $K_p = 1.99$, $K_i = 0.98$, $K_d = 1.35$, and for SMS-EMOA $K_p = 2.35$, $K_i = 0.96$, $K_d = 1.97$.

Table 7.6: PID parameters in Figure 7.8.

Algorithm	B2	B1	B0
EHVI-EGO	$\begin{bmatrix} -146.8052 & -183.1330 \\ -39.5844 & 38.28307 \end{bmatrix}$	$\begin{bmatrix} -58.8757 & -39.9390 \\ 39.1692 & 164.6072 \end{bmatrix}$	$\begin{bmatrix} -29.1297 & 168.1379 \\ 11.2049 & 148.3339 \end{bmatrix}$
THEIV-EGO	$\begin{bmatrix} -110.9551 & 197.8837 \\ 198.4738 & 199.5100 \end{bmatrix}$	$\begin{bmatrix} 45.5191 & 194.3873 \\ 80.6678 & -188.7033 \end{bmatrix}$	$\begin{bmatrix} -30.7334 & 151.2778 \\ 76.1469 & 35.5006 \end{bmatrix}$
NSGA-II	$\begin{bmatrix} -68.0186 & 199.9837 \\ 83.4419 & 21.5003 \end{bmatrix}$	$\begin{bmatrix} -15.0820 & 199.8181 \\ 117.6667 & 200 \end{bmatrix}$	$\begin{bmatrix} 74.1652 & 139.4757 \\ 58.1943 & 94.3620 \end{bmatrix}$
SMS-EMOA	$\begin{bmatrix} -44.6694 & 198.9674 \\ 113.6318 & 198.1877 \end{bmatrix}$	$\begin{bmatrix} -123.9725 & 69.6727 \\ -44.6645 & 149.6474 \end{bmatrix}$	$\begin{bmatrix} -34.5741 & 158.8530 \\ -10.7696 & 116.9635 \end{bmatrix}$

Figure 7.8 shows the step response with plant perturbation, and the PID param-

eters are shown in Table 7.6. The objective values for each method are: EHVI-EGO = (2.1264, 0.5646), TEHVI-EGO= (2.1391, 0.1023), NSGA-II = (2.1722, 0.9990) and SMS-EMOA=(2.1707, 0.9991). It is clear that the EGO-based controller outputs are slightly better than those generated by the other two algorithms. For output y_2, the overshoot of the TEHVI-EGO step response is bigger than the other three responses. This is acceptable, considering that the objective functions do not have the overshoot criterion, and the overshot is also less than 20%.

7.4.3 Bio-plant Optimization

For the bio-gas plant, two strategies of setting reference point are used: fixed and dynamic reference points. The fixed reference point is always (0.1, 1.6), while, the dynamic reference point is determined on the fly by the algorithm and is calculated by adding one to the maximum value of the existing Pareto fronts. The initial substrate feeds and parameters in the experiments are represented in Table 7.3. Bio-gas plant simulation costs a lot of time (about 15-24 hours), and thereby, we did the experiments only once.

Figure 7.9 illustrates the final intermediate Pareto fronts with dynamic reference point and initial substrate feeds of experiments A and C, respectively.

In Figure 7.9, nearly all elements in the SMS-EGO and SMS-EMOA intermediate Pareto fronts are dominated by those in EHVI-EGO intermediate Pareto fronts. When compared the performance of SMS-EGO with that of SMS-EMOA, SMS-EMOA is a little bit better than SMS-EGO at the cost of 150, 525 and 300 more evaluations in Exp. 1&7, 2&8 and 3&9, respectively. The choice of the reference point is very important in these experiments. The HV differs a lot when choosing different reference points. Take an example in Figure 7.9 (a). When compared the red and blue Pareto fronts in the right subfigure, only one element in EHVI-EGO Pareto front is dominated by that of SMS-EGO, and HV for A3 and A6 are 0.1381 and 0.1584, respectively with the same reference point of (-1.8, 0.7). However, HV for A3 and A6 are 3.3995 and 3.3758 using the reference point of (0.1, 1.6). Hence, the criterion of HV is very sensitive to the reference point, and the bad choice of reference point can mislead the final decision, even when the results are very clear.

Figure 7.10 shows the steady Pareto front in Exp. A and C. The performance gap between all the three algorithms is not obvious. Even some few elements in the Pareto front, generated by EHVI-EGO, are dominated by those of SMS-EMOA and SMS-EMOA. When compared the intermediate with steady Pareto fronts us-

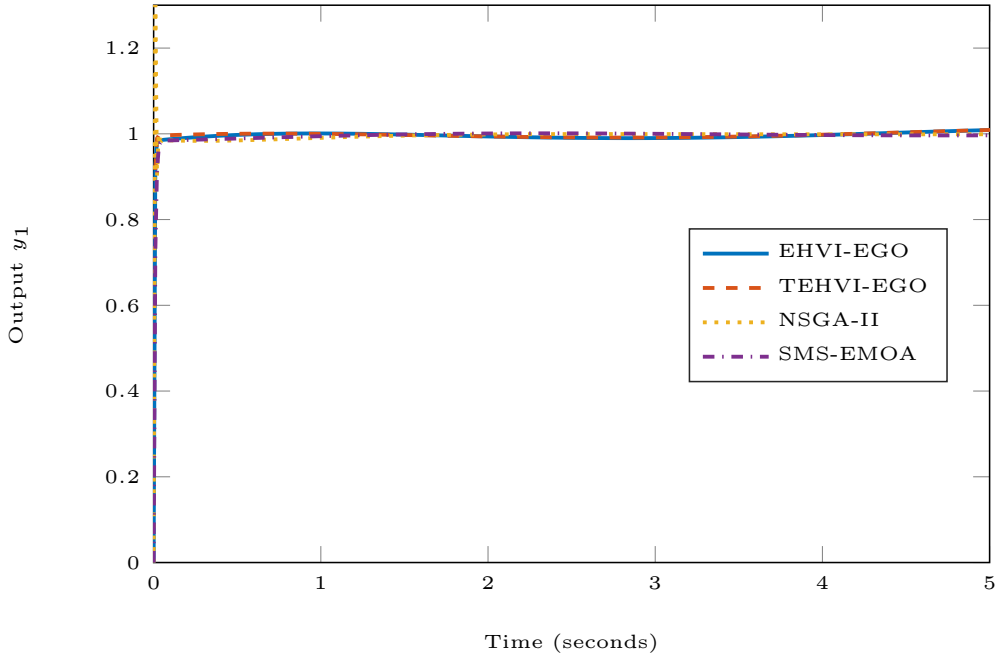

(a) The step response for output y_1.

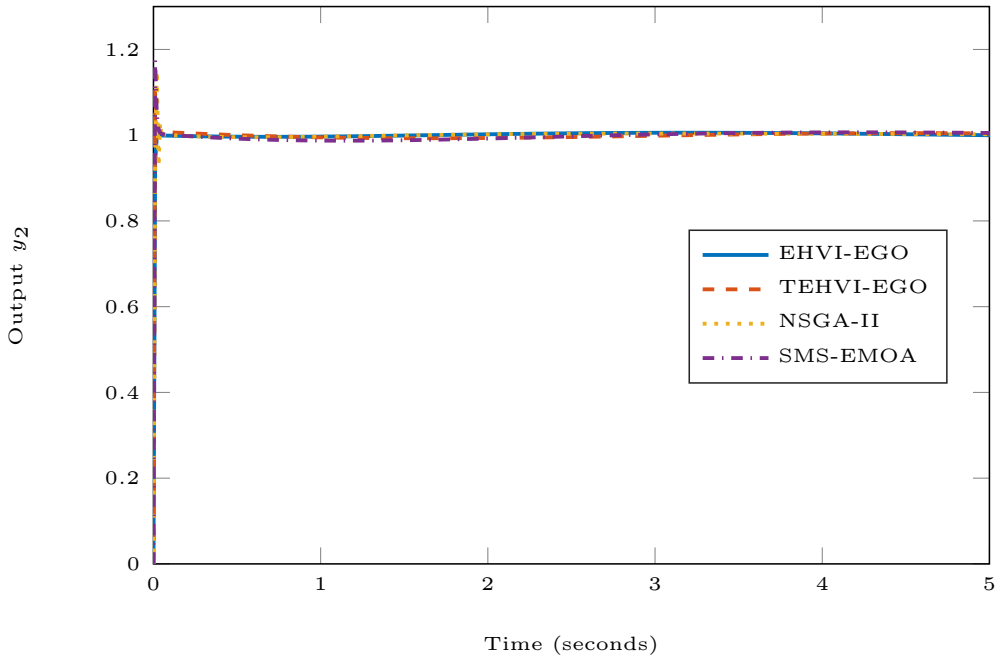

(b) The step response for output y_2.

Figure 7.8: Step responses.

(a) Final intermediate Pareto fronts in Exp. A with dynamic reference point.

(b) Final intermediate Pareto fronts in Exp. C with dynamic reference point.

(c) Steady Pareto fronts in Exp. A with dynamic reference point.

(d) Steady Pareto fronts in Exp. C with dynamic reference point.

Figure 7.9: Experimental results on Exp. A & C, using dynamic reference point strategy.

ing a dynamic reference point, the performance gap of the three algorithms diminished for steady state. That is to say, the predictions by surrogate-model-based algorithms still process a slight difference to the real data, for steady state.

Figure 7.10 (a) and (b) are both the intermediate Pareto fronts using a fixed reference point with different initial substrate feed strategies (A and B). Figure 7.10 (c) and (d) are the steady Pareto fronts based on fixed reference point.

For the fixed reference point strategy, the performance of EHVI-EGO is similar to SMS-EGO. The reason of this could be the bad choice of the reference point. Some actual better Pareto fronts are regarded as the worse ones in process optimization, due to the improper reference point. However, it still needs more experiments to verify this assumption.

Comparing all the intermediate Pareto fronts with a dynamic and fixed reference point, EHVI-EGO outperforms SMS-EGO when using a dynamic reference point, while SMS-EGO is better than EHVI-EGO when using a fixed reference point. This means that SMS-EGO is more robust against the choice of a reference point than EHVI-EGO. Another evidence of this conclusion can be found in Table 7.7: the number of elements in EHVI-EGO intermediate Pareto front is always smaller than that of SMS-EGO, and EHVI-EGO standard deviation is larger than SMS-EGO's.

Table 7.7: Number of elements in intermediate Pareto fronts.

		EHVI-EGO				SMS-EGO			
Ref.	Exp.	AVG	MIN	MAX	σ	AVG	MIN	MAX	σ
Dynamic	A	14.51	6	23	4.04	20.49	7	27	5.09
Dynamic	C	16.71	5	28	5.86	21.87	11	35	5.34
Fixed	A	19.29	7	33	8.15	22.53	11	31	4.50
Fixed	B	16.04	9	24	3.38	20.73	8	29	6.45

Contrary to PID parameter tuning, the Pareto fronts in a bio-gas plant are more similar. This is because the total function evaluations numbers within the simulation in the bio-gas plant are much larger than the corresponding ones in PID parameter tuning. For the bio-gas plant, $T_p = 150$, $T_c = 10$ and n_{eval} is the function evaluation number in each control period. Therefore, the total function evaluations number in the whole simulation period is 15 times n_{eval}.

(a) Intermediate Pareto fronts in Exp. A with fixed reference point.

(b) Intermediate Pareto fronts in Exp. B with fixed reference point.

(c) Steady Pareto fronts in Exp. A with fixed reference point.

(d) Steady Pareto fronts in Exp. B with fixed reference point.

Figure 7.10: Experimental results on Exp. A & B, using fixed reference point strategy.

7.5 Summary

In this chapter, we investigated different evolutionary multi-criterion optimization algorithms for the optimization of PID controllers and bio-gas plants optimization. The focus of our study was hypervolume based methods for problems that allow only a small (≈ 100) number of exact objective function evaluations. In particular, a state-of-the-art evolutionary algorithm (SMS-EMOA) was compared to multi-objective efficient global optimization algorithms, SMS-EGO and EHVI-EGO, which utilize a surrogate model of the objective functions. In the problem domain of PID controller tuning, the results were, as expected, that the surrogate model assisted strategies yielded better results than the SMS-EMOA. Among them, the EHVI-EGO performs slightly better than the SMS-EGO, but it is more sensitive to the change of the reference point.

However, in the case of the optimization of the bio-gas plant, the result seems to be less consistent. While also in this case, for intermediate control optimization the EHVI-EGO shows the best performance, there is no big gap between all the algorithms performances. Also the SMS-EMOA, which uses no surrogate model, manages to produce a diverse Pareto-front that in terms of convergence is only slightly worse than that of EHVI-EGO. More surprisingly, the gap between the algorithms performances almost diminishes when it comes to applying the optimized control in steady state. The consistency of the results by the three algorithms shows that the solution is probably close to the true Pareto front.

Between EHVI-EGO and TEHVI-EGO, TEHVI-EGO outperforms EHVI-EGO in the case of robust PID tuning problem, as the TEHVI only considers the EHVI in a certain domain, and therefore, it can force the algorithm on exploring in this domain. Summarizing, based on the result of this study we recommend using TEHVI-EGO when the a-priori knowledge of the objective functions is available. Otherwise, we recommend to use EHVI-EGO, because it shows a good performance more consistently as compared to the other algorithms. For further work, it is recommended to research the robust setting for the reference point.